Flame-coating of titania particles with silica

A. Teleki, S.E. Pratsinis,[a] K. Wegner, and R. Jossen
Particle Technology Laboratory, Institute of Process Engineering, Department of Mechanical and Process Engineering, Swiss Federal Institute of Technology Zurich (ETHZ), CH-8092 Zurich, Switzerland

F. Krumeich
Laboratory of Inorganic Chemistry, Department of Chemistry and Applied Biosciences, Swiss Federal Institute of Technology Zurich (ETHZ), CH-8093 Zurich, Switzerland

(Received 2 November 2004; accepted 18 February 2005)

Silica/titania composite particles were prepared by co-oxidation of titanium-tetra-isopropoxide and hexamethyldisiloxane in a co-flow diffusion flame reactor. The influence of precursor composition on product powder characteristics was studied by x-ray diffraction, nitrogen adsorption, electron microscopy, elemental mapping, and energy-dispersive x-ray analysis. The flame temperature was measured by Fourier transform infrared spectroscopy. The evolution of composite particle morphology from ramified agglomerates to spot- or fully coated particles was investigated by thermophoretic sampling and transmission/scanning electron microscopy. At 40–60 wt% TiO_2, particles with segregated regions of silica and titania were formed, while at 80 wt% TiO_2 rough silica coatings were obtained. Rapid flame-quenching with a critical flow nozzle at 5 cm above the burner nearly halved the product particle size, changed its crystallinity from pure anatase to mostly rutile and resulted in smooth silica coatings on particles containing 80 wt% TiO_2.

I. INTRODUCTION

Flame technology is used to produce large quantities of oxide nanoparticles and carbon black.[1] For instance, half of the global annual production of pigmentary titania (~2 million tons) is made by $TiCl_4$ oxidation in flame reactors.[2] Titania particles, in particular, possess a combination of attractive optical properties such as absorption and scattering of ultraviolet (UV) light and a very high refractive index[3] that make them attractive in sunscreens for protection against UVA and UVB.[4] Titania embedded in a polymer matrix is of great interest in fabrication of UV filters, coatings for UV-sensitive materials, and lenses.[3,5] However, titania is also photocatalytically active when exposed to UV-light. To prevent degradation of the matrix by the embedded titania particles, their surface should be passivated, for instance, by SiO_2 coating.[6] This is of importance in sunscreen applications as radiation absorption results in reactive species that may even damage the skin tissue.[7]

Flame-made titania pigments are typically coated in a post-synthesis, wet-phase treatment: nanosized hydrous oxides of Al, Zr, Sn or Si are precipitated onto the surface of titania, according to a process pioneered by DuPont in the 1960s.[2,8,9] The applied coatings can improve the degree of pigment dispersion also, as nanosized asperities are formed on the particle surface preventing agglomeration. Silica coating of titania, in particular, yields maximum powder durability but is accompanied by loss of opacity. This is mainly a consequence of agglomeration during wet-phase treatment[10] requiring an additional milling step for agglomerate breakage.[11] Furthermore, wet dispersion of the starting powder, filtration, washing, and drying add to production, maintenance, and pollution control costs of the wet-phase post-treatment. The control of the coating morphology is also difficult in the precipitation process.[12] Rough and porous coatings are often obtained whereas denser coatings are desired to improve pigment durability and to obtain maximum reduction in photoactivity.

Product powder morphology, such as coating density and particle agglomeration, might be more easily controlled by gas-phase coating during particle synthesis. Piccolo et al.[13] dry-coated titanium dioxide pigments suspended in a carrier gas in a tubular reactor by injection of aluminum or silicon halides. Santacesaria et al.[14] fed $SiCl_4$ vapor into a fluidized bed of solid titanium dioxide pigments, forming compact and coherent coatings. Akhtar et al.[15] observed silica enrichment on the surface of titania particles made by $TiCl_4$ oxidation in the presence of $SiCl_4$ in a hot-wall flow reactor. Hung and Katz[16]

[a]Address all correspondence to this author.
e-mail: pratsinis@ptl.mavt.ethz.ch
DOI: 10.1557/JMR.2005.0160

Downloaded from https://www.cambridge.org/core. University of Basel Library, on 30 May 2017 at 20:04:30, subject to the Cambridge Core terms of use, available at https://www.cambridge.org/core/terms. https://doi.org/10.1557/JMR.2005.0160

produced silica coatings 10–40 nm thick on 30–40 nm particles containing 30–60 wt% TiO_2 by co-oxidation of $TiCl_4$ and $SiCl_4$ in oxy-hydrogen counterflow diffusion flames. Increasing the maximum temperature in these flames from 2300 to 2800 K resulted in discrete silica particles attached on titania rather than coatings. Silica coatings were formed at ≤60 wt% TiO_2 by co-oxidation of $SiCl_4$ and $TiCl_4$ in diffusion flame reactors.[17] Kodas et al.[18] synthesized titania by $TiCl_4$ oxidation in a hot-wall aerosol flow reactor and introduced Si-, Al-, or Zr-containing precursors downstream from the particle formation zone to produce oxide coatings on the titania nanoparticles. Powell et al.[19] produced titania particles with an average size of 0.8 μm from $TiCl_4$ and applied silica coatings 5–100 nm thick by introducing $SiCl_4$ at various concentrations into the hot-wall reactor (5–60 wt% TiO_2). Smoother and more uniform coatings were obtained at higher reactor temperatures. Ehrman et al.[20,21] produced SiO_2/TiO_2 powders (15–90 wt% TiO_2) from $SiBr_4$, $SiCl_4$, or hexamethyldisiloxane (HMDSO) and $TiCl_4$ in premixed flames and observed segregated silica/titania phases. Varying the mixing modes of silica and titania precursors in a tubular furnace, Lee et al.[22] made SiO_2/TiO_2 particles, including core-shell and mixed type structures containing 20–100 wt% TiO_2.

Despite its significance, silica coating of TiO_2 remains a challenge, in particular, the formation of smooth coatings during flame synthesis of TiO_2, which is an established industrial process. Here, co-flow diffusion flame reactors, which are commonly used for nanoparticle production,[23] are used in synthesis of silica/titania nanoparticles over a range of titania mass fractions. Process conditions for silica-coated titania were identified. The dynamic evolution of the silica coating morphology was studied by thermophoretic sampling and electron microscopy. The effect of rapid flame quenching[24] on silica/titania particle morphology was investigated.

II. EXPERIMENTAL

A. Particle synthesis and flame diagnostics

Figure 1 shows a schematic illustration of the experimental setup. A co-flow diffusion flame aerosol reactor consisting of three concentric stainless-steel tubes was used.[25] An argon stream of 0.75 l/min carrying distilled titanium-tetra-isopropoxide (TTIP; Aldrich, Buchs, Switzerland, purity >97%) vapor was introduced through the center tube of the burner along with 0.5 l/min methane carrying distilled hexamethyldisiloxane (HMDSO, Sigma-Aldrich, Buchs, Switzerland, purity >99%) vapor. Through the second tube of the burner (first annulus) 0.50 l/min nitrogen was flowing to prevent particle deposition on the burner rim while 2 l/min oxygen was provided through the third tube (second annulus). All gas (Pan Gas, Luzern, Switzerland, purity >99.999%) flow

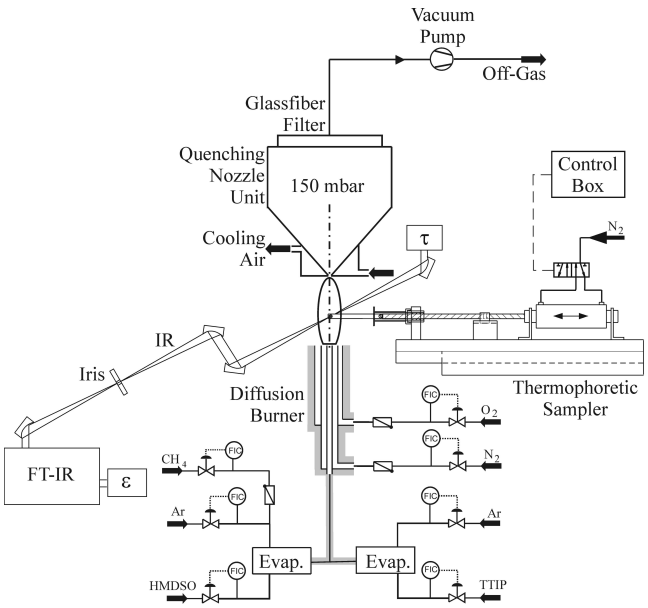

FIG. 1. Schematic illustration of the experimental setup with the gas and precursor delivery system, co-flow diffusion burner, glass fiber filter and filter holder, FTIR spectrometer for flame temperature measurements, and thermophoretic sampler for particle collection on TEM grids. The expansion nozzle was connected to the filter holder and placed at 5 cm above the burner.

rates were controlled by calibrated mass flow meters (Bronkhorst EL-flow F201, Ruurlo, The Netherlands). Evaporators (Bronkhorst, CEM 100 W) and liquid mass flow meters (Bronkhorst, Liqui-Flow) were used to deliver a constant stream of precursor vapors.[25] The evaporators, burner, and all reactant delivery tubes were heated to 175 °C to prevent precursor condensation.

Product particles were collected 30 cm above the end of the luminous part of the flame with the aid of a vacuum pump (Vacuubrand RZ 16, Wertheim, Germany) on a glass fiber filter (Whatman Springfield Mill, Maidstone, Kent, UK, GF/A) placed in a stainless steel filter holder. An expansion nozzle 0.15 cm in diameter could be connected to the filter holder to form a gas expansion—particle collection unit, which was positioned 5 cm above the burner.[25] Silica/titania powders containing 0–100 wt% TiO_2 were produced with and without that nozzle at constant 5 g/h production rate by varying the inlet precursor composition.

A Fourier transform infrared (FTIR) spectrometer (Bomem MB155S, Quebec, Canada) operated over the spectral range of 6500–500 cm^{-1} with a resolution of 4 cm^{-1} and a 0.2 cm infrared (IR) beam diameter was used to measure the temperature of the unquenched and nozzle-quenched flames with and without addition of precursors.[26] Emission (radiance) and transmission (or background) spectra were collected with a wide-band deuterated-triglycine-sulfate (DTGS) detector and a liquid nitrogen cooled mercury-cadmium-telluride (MCT) detector, respectively. For each temperature 128 scans

Downloaded from https://www.cambridge.org/core. University of Basel Library, on 30 May 2017 at 20:04:30, subject to the Cambridge Core terms of use, available at https://www.cambridge.org/core/terms.
https://doi.org/10.1557/JMR.2005.0160

for the transmission, 64 scans for the emission (blackbody and radiance) and 32 scans for the background spectra were collected and analyzed. Flame temperatures were evaluated while the spectrometer and detector performance was validated by reproducing (±25 K) the temperature profile of a premixed flame (Fig. 5 in Kammler et al.[26]). It should be noted that FTIR uses an integral line-of-sight through the whole flame. Thus, FTIR averages the lower CO_2 temperatures found at the flame edge with higher temperatures in the flame center.[26] This can be overcome by tomographic reconstruction of the line-of-sight measurements to obtain locally resolved radiance and transmittance spectra, as was demonstrated by Kammler et al.[26] for a premixed flame. In the lower parts of the premixed flat flame, where the temperature is uniform, excellent agreement of the tomographic reconstruction with the line-of-sight measurements was found. At higher positions, flame edge effects are more significant, and the temperature was increased by maximum 100 K by the tomographic reconstruction technique. In the present study, it would not be possible to apply the tomographic reconstruction technique, as the IR beam diameter was 2 mm while the flame thickness was <10 mm, e.g., not thick enough to provide sufficient measurement points for the tomographic reconstruction.

B. Particle sampling and analysis

Particles were collected by filtration and by thermophoretic sampling (Fig. 1) on transmission electron microscopy (TEM) grids at various heights above the burner (HAB = 1, 3, 5 and 15 cm) within 50 ms.[27] High-resolution transmission electron microscopy (HRTEM; Philips Tecnai F30, field emission cathode, 300 kV, FEI, Eindhoven, The Netherlands) was used to determine the particle and coating morphology. By electron spectroscopic imaging (ESI), elemental maps of Ti and Si were recorded with a Gatan Imaging Filter (GIF, Munich, Germany) mounted below the TEM column. Scanning transmission electron microscopy (STEM) images were recorded with a high-angle annular dark-field detector (HAADF, FEI). The concentration of each element at selected spots in the STEM images was determined by energy-dispersive x-ray (EDX) analysis (Fa.EDAX detector, Taunusstein, Germany).

The particle Brunauer–Emmett–Teller (BET) specific surface area (SSA) was measured by nitrogen adsorption at 77 K (Micromeritics TriStar 3000, Norcross, GA). Assuming all particles to be monodispersed spheres, the BET equivalent diameter was calculated as $d_{BET} = 6/(\rho_{TiO_2/SiO_2} \times SSA)$ with the density $\rho_{TiO_2/SiO_2} = x \times \rho_{TiO_2} + (1 - x) \times \rho_{SiO_2}$, x the mass fraction of TiO_2, $\rho_{SiO_2} = 2200$ kg/m^3 and $\rho_{TiO_2} = 4260$ or 3840 kg/m^3 for rutile or anatase.

Absorption spectra (applying the Kubelka–Munk equation) of the silica/titania powders, in the wavelength range of 190–400 nm, were recorded with a UV–visible–near-infrared (UV-vis-NIR) spectrometer (Varian, Cary 500, Mulgrave, Australia). Diluted samples for the analysis were prepared by grinding 20 mg powder together with 80 mg barium sulfate ($BaSO_4$; Riedel-de Haën, Seetze, Germany, extra pure). Spectra of pure barium sulfate were recorded and used for baseline correction of the SiO_2/TiO_2 spectra.

X-ray diffraction (XRD) patterns of product powders were obtained with a Bruker D8 (Karlsruhe, Germany) advance diffractometer operating with Cu K_α radiation. Crystallite size and phase composition were obtained using the Rietveld method and the fundamental parameter approach.[28]

III. RESULTS AND DISCUSSION

A. Flame characterization

Figure 2 shows the line-of-sight temperature profiles along the burner axis (centerline) of the co-flow CH_4/O_2 diffusion flames without (filled symbols) and with (open symbols) the flame-quenching nozzle at 5 cm above the burner. Flame temperatures were measured in the absence of particles (circles), as well as in flames producing 5 g/h of either pure SiO_2 (6.5 g/h HMDSO; triangles) or 80 wt% TiO_2 (1.4 g/h HMDSO and 13.5 g/h TTIP; diamonds). All flames reach a maximum temperature of about $T_{max} = 2450$ K at 1.8 cm above the burner. The temperature of the unquenched, particle-free flame (filled circles) remains nearly constant at T_{max} up to 5 cm above the burner and then decreases almost linearly to 650 K at 20 cm HAB. Particle-laden, unquenched flames are slightly hotter and their visible lengths are longer than that of the particle-free (CH_4) flame. Compared to the latter flame ($\Delta H_{c,CH^4} = -803$ kJ/mol),[29] the enthalpy

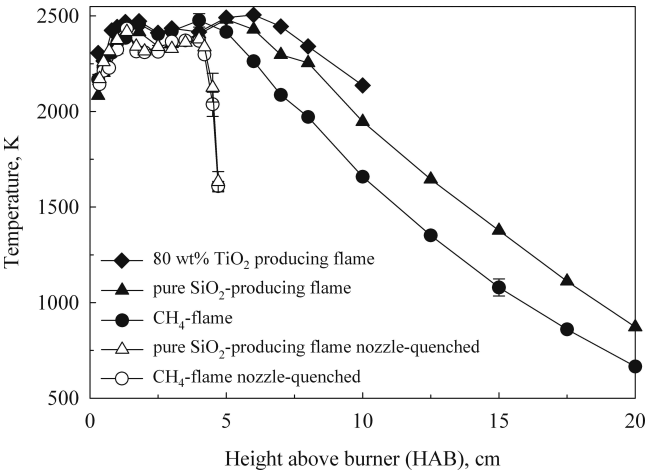

FIG. 2. Average flame temperature along the burner axis (centerline) as a function of height above burner (HAB) for unquenched (filled symbols) and nozzle-quenched (open symbols) CH_4 (0.5 l/min)/O_2 (2 l/min) co-flow diffusion flames without precursor (circles), as well as producing pure silica (triangles) and 80 wt% TiO_2 (diamonds). The flame temperature decreases by 750 K in front of the quenching nozzle.

Downloaded from https://www.cambridge.org/core. University of Basel Library, on 30 May 2017 at 20:04:30, subject to the Cambridge Core terms of use, available at https://www.cambridge.org/core/terms.
https://doi.org/10.1557/JMR.2005.0160

content of the flame increases by 20% for the pure SiO_2 particle-laden ($\Delta H_{c,HMDSO} = -5540$ kJ/mol)[29] and by 40% for the 80 wt% TiO_2 particle-laden flames ($\Delta H_{c,TTIP} = -8088$ kJ/mol).[25] These temperature profiles and maximum values are consistent with Mueller et al.[30] who produced 9 g/h SiO_2 at the same burner configuration and similar conditions.

Up to 1.8 cm HAB, the temperature profiles of the nozzle-quenched flames are essentially identical to the unquenched ones at T_{max} while they are about 100 K lower than the unquenched flames up to 4 cm HAB (1 cm in front of the nozzle) which is within the FTIR accuracy. Above 4 cm HAB, the temperature of the nozzle-quenched flames drops rapidly by about 100 K/mm and reaches 1600 K at HAB = 4.7 cm (0.3 cm in front of the nozzle) regardless of particle content. This steep temperature reduction is attributed to mixing with ambient air drawn into the nozzle resulting in 900 K at 0.8 cm downstream of the nozzle.[25]

Figure 3 shows the absorbance spectra of the gases of the unquenched flame at various HAB for production of 5 g/h 80 wt% TiO_2 particles. The intensities of the absorption bands of CH_4, HMDSO, and TTIP (3016, 2900, 1306, 1132, 1008, 850, and 650–670 cm^{-1})[31] decrease with increasing HAB and are no longer visible at 3 cm HAB. This indicates that CH_4, HMDSO, and TTIP are completely converted at this HAB.[30] This is at the maximum temperature region of the flame (Fig. 2). Accordingly, the intensity of the peaks arising from bond vibrations[32] in CO_2 (2349 cm^{-1}), H_2O (3000–3500 cm^{-1}) and TiO_2 (650–670 cm^{-1}) increases as the combustion proceeds, especially that for CO_2 and TiO_2.

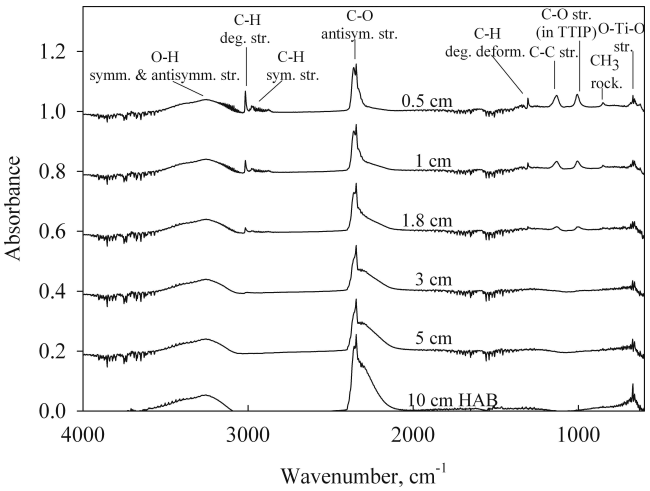

FIG. 3. FTIR absorption spectra of the flame producing 80 wt% TiO_2 at various HAB. The spectra are shifted by 0.2 for better visualization. The assignment of the main vibrational groups in the spectra are shown (antisym.: antisymmetric, deform.: deformation, deg.: degenerate, rock.: rocking, str.: stretching, and sym.: symmetric). At 3 cm HAB absorption bands arising from vibrational groups in the fuels (TTIP, HMDSO, and CH_4) are no longer visible.

B. Unquenched flame synthesis of SiO_2/TiO_2

1. Effect of composition on particle morphology

Figure 4 shows TEM images of silica/titania particles made with the unquenched flame: (a) pure SiO_2, (b) 20 wt%, (c) 40 wt%, (d) 60 wt%, (e) 80 wt%, and (f) 100 wt% TiO_2. For all compositions, the particles are mostly spherical with a low degree of agglomeration. At the high temperatures and short residence times (~10 ms) encountered in these flames, most particles fully coalesce upon collision forming spherical ones. Pure silica [Fig. 4(a)] forms spherical or nearly spherical particles with sintering necks discernible between some of the particles.[30] Similarly, sintering necks between some of the particles containing 20 wt% TiO_2 are discernible [Fig. 4(b)].

No distinct titania domains are TEM-visible in the particles containing 20 wt% TiO_2 [Fig. 4(b)] consistent with Ehrman et al.[21] who produced 14 wt% TiO_2 particles in a premixed flame. Stakheev et al.[33] prepared SiO_2/TiO_2 powders by precipitation and found homogeneous solid solutions of Ti^{4+} in SiO_2 at $\leqslant$10 wt% TiO_2. A blue-shift in the absorption spectrum (bandgap energy: 3.92 eV) was observed for the 20 wt% TiO_2 powder. Compared to pure titania (3.36 eV), this indicates small titania domains[34] that might not be discernible by TEM. Silica-titania interactions can also contribute to the observed increase in the bandgap energy.[35]

In most 40 wt% TiO_2 particles amorphous (light) and crystalline (dark) regions can be discerned, indicating segregated regions of amorphous silica and crystalline titania [Fig. 4(c)]. This is confirmed by a HRTEM image made at a higher magnification [Fig. 5(a)]. Here, lattice planes are clearly visible indicating regions of crystalline titania, next to an amorphous region. At 60 wt% TiO_2 [Fig. 4(d)] phase segregation is again observed, the crystalline regions are larger than those in particles with 40 wt% TiO_2 [Fig. 4(c)]. Powders with both 40 and 60 wt% TiO_2 also contain particles of either pure silica or pure titania [Figs. 4(c) and 4(d)]. The formation of segregated regions of silica and titania reduces the free energy of the system.[21] In the solid phase, no thermodynamically favorable mixed oxide phase of SiO_2 and TiO_2 exists.[36] Phase segregation as predicted by the phase diagram was also observed by Ehrman et al.[21] in flame-made silica/titania particles with 20–90 wt% TiO_2 and by Stakheev et al.[33] in wet-made silica/titania particles with 10–85 wt% TiO_2. Schultz et al.[37] experimentally observed, however, the solubility of titania in silica glasses containing up to 12 wt% TiO_2. Above 2000 K titania is soluble in silica up to 20 wt% TiO_2. At higher mass fractions of titania, the oxides exist as two immiscible liquids.[36]

Silica coatings on the titania particle surface are observed for some particles containing 80 wt% TiO_2,

Downloaded from https://www.cambridge.org/core. University of Basel Library, on 30 May 2017 at 20:04:30, subject to the Cambridge Core terms of use, available at https://www.cambridge.org/core/terms.
https://doi.org/10.1557/JMR.2005.0160

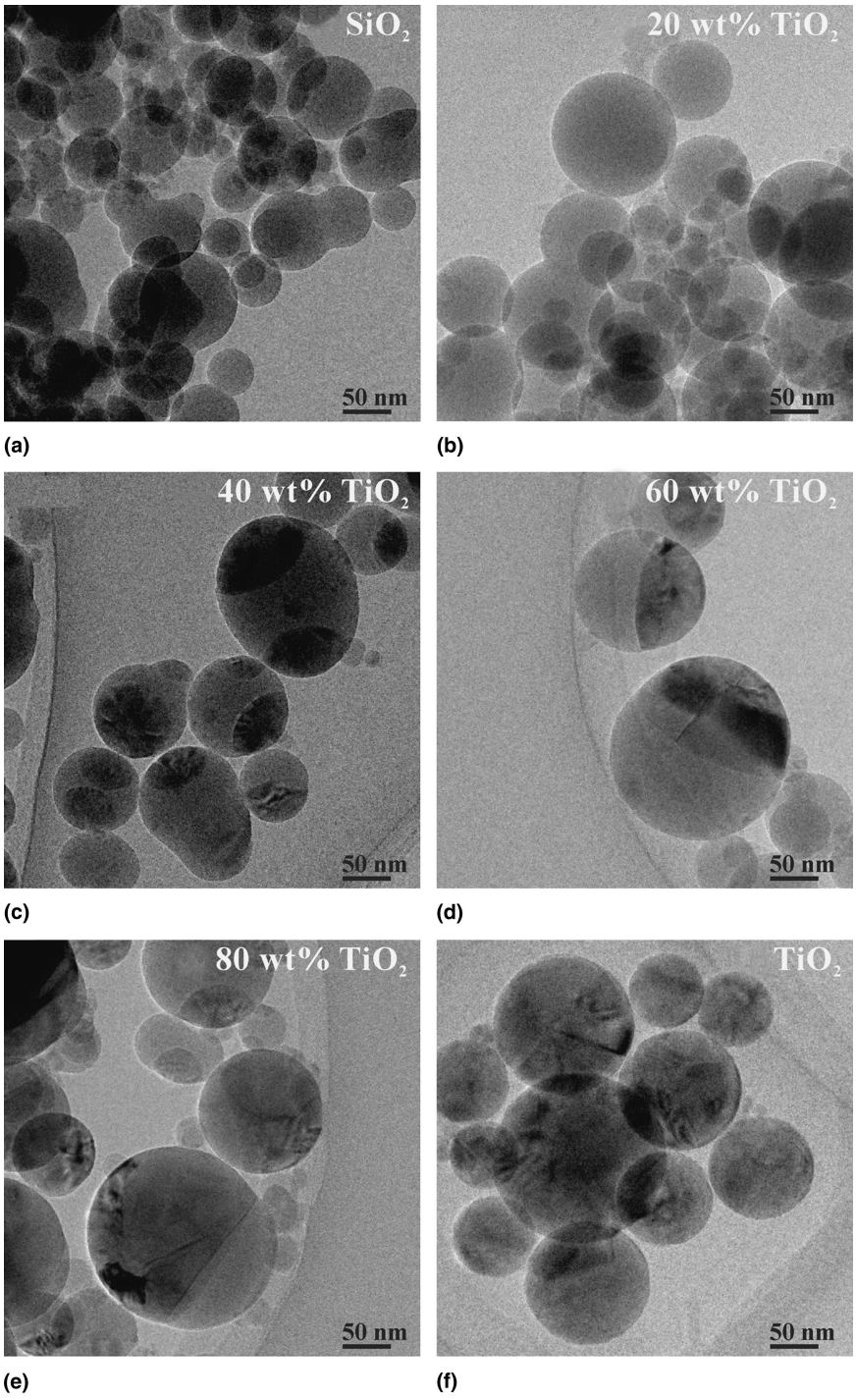

FIG. 4. TEM images of (a) pure silica, (b) 20 wt% TiO_2, (c) 40 wt% TiO_2, (d) 60 wt% TiO_2, (e) 80 wt% TiO_2, and (f) pure titania produced without the quenching nozzle. Particles with 40 and 60 wt% TiO_2 have segregated regions of silica and titania, coated particles can be seen at 80 wt% TiO_2.

though phase segregation within most of the particles dominates [Fig. 4(e)]. A HRTEM image at higher magnification shows a TiO_2 particle encapsulated by a layer of silica [Fig. 5(b)]. A smooth coating layer 2–10 nm thick fully encapsulates the particle. In contrast to the 40 or 60 wt% TiO_2 powders, the segregation of the two oxides occurs also on the surface and not solely within the particles containing 80 wt% TiO_2. This is consistent with Powell et al.[19] who observed that decreasing the silica concentration resulted in SiO_2 coatings on TiO_2 rather than separate SiO_2 particles.

Coated particles could form as a result of differences

Downloaded from https://www.cambridge.org/core. University of Basel Library, on 30 May 2017 at 20:04:30, subject to the Cambridge Core terms of use, available at https://www.cambridge.org/core/terms.
https://doi.org/10.1557/JMR.2005.0160

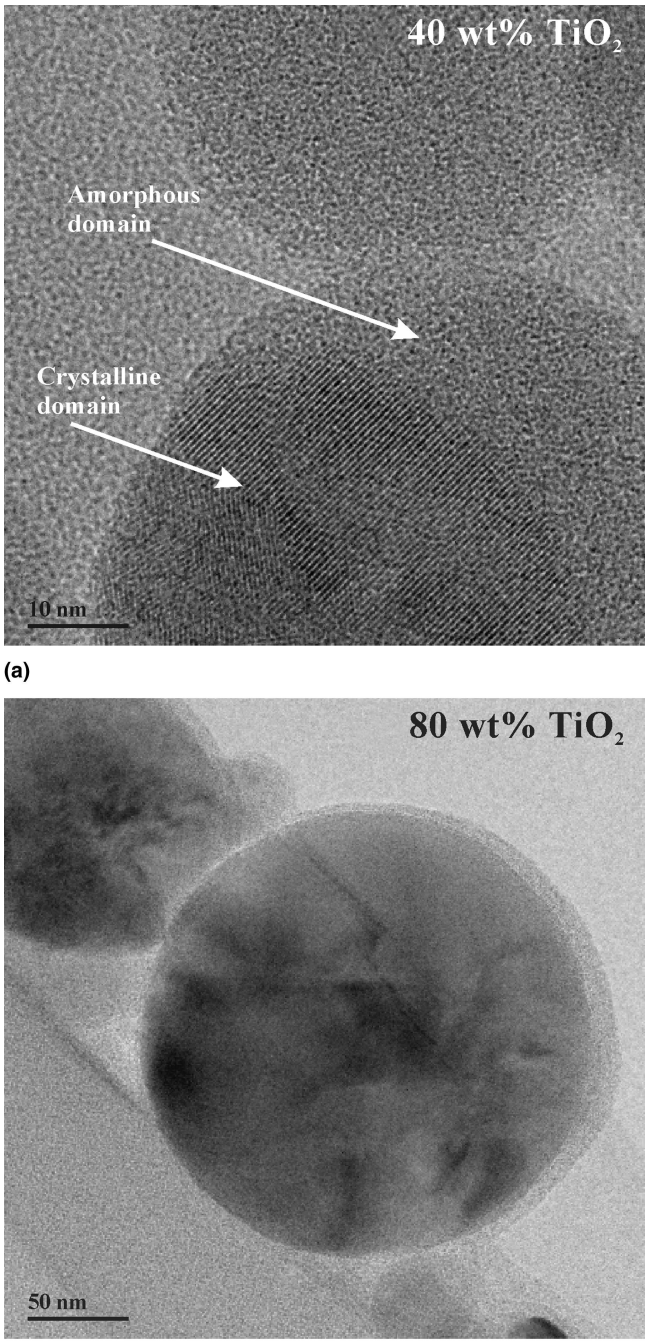

FIG. 5. HRTEM images of particles with (a) 40 wt% TiO_2 and (b) 80 wt% TiO_2. Lattice planes indicating crystalline titania are visible next to an amorphous region (silica) in the 40 wt% TiO_2 particle. A titania particle encapsulated by silica is seen at 80 wt% TiO_2.

in the chemical reaction rates of the precursors.[16,17,20] For example, the oxidation rate of $TiCl_4$ is much faster than that of $SiCl_4$ and silica formed from $SiCl_4$ deposits on titania particles formed at lower temperatures.[16] This was observed in co-flow[17] and counter-flow[16] diffusion flames ($\geq$60 wt% TiO_2).

2. Evolution of SiO_2 coating morphology on TiO_2

The evolution of the formation of particles containing 80 wt% TiO_2 [Fig. 4(e)] was further investigated. Figure 6 shows TEM images of these particles that were thermophoretically sampled at 1, 3, 5, and 15 cm HAB. Fractal-like particles as well as single spherical particles can be seen at HAB = 1 cm [Fig. 6(a)]. Particles with both a crystalline titania region (dark), and an amorphous region (light) indicating silica are also visible. Regions rich in Ti and Si were verified by EDX in particles with dark and light regions, respectively. Larger spherical particles contained mainly titania. The nonuniformly shaped particles may come from partially combusted precursors deposited at the TEM grid at HAB = 1 cm that were converted to oxides after collection.[38] Recall that precursor conversion is completed later on, HAB = 3 cm (Fig. 3).

In synthesis of 80 wt% TiO_2 particles, oxidation of the more concentrated TTIP proceeds faster than that of HMDSO forming larger spherical particles of titania and small silica agglomerates [Fig. 6(a)]. Titania sinters faster than silica at these temperatures.[39] At the low HMDSO concentration, few and small SiO_2 particles and/or aggregates will be formed which collide or deposit on the TiO_2 particles. Hence, silica particles are attached to the titania surface [Fig. 6(a)] where they may sinter. Alternatively, HMDSO could react directly on the titania surface.[40]

Particles grow further by coagulation and coalescence through the high temperature region (up to HAB = 6 cm) of the flame (Fig. 2). Particles sampled at HAB = 3 cm [Fig. 6(b)] are larger than those at 1 cm [Fig. 6(a)]. Less agglomerates but more spherical particles exist at 3 cm HAB [Fig. 6(b)], while at 5 cm HAB all particles have fully coalesced and no agglomerated are observed [Fig. 6(c)]. At 3 cm HAB, individual spherical or agglomerate particles of either titania or silica exist, as well as many particles with segregated regions of silica and titania [Fig. 6(b)]. At 5 cm HAB separate silica regions on the surface are discernible as was confirmed by EDX and elemental mapping [Fig. 6(c)].

Most particles sampled 15 cm above the burner are either individually coated spherical ones or have distinct SiO_2 and TiO_2 regions [Fig. 6(d)]. Here, the flame temperature has dropped significantly (Fig. 2) and particle growth has ceased. Particle sizes observed by TEM at 15 cm HAB [Fig. 6(d)] are comparable to the ones collected on the filter [Fig. 4(e)]. In some particles, silica, which was observed as separate islands on the surface of titania at 5 cm HAB, has fused on the surface forming thinner coating layers. The coating thickness on these entirely encapsulated titania particles is about 2–5 nm, in agreement with coating thicknesses observed in the powders collected on the filter [Fig. 5(b)].

The filamentary SiO_2 formed at early stages in the

Downloaded from https://www.cambridge.org/core. University of Basel Library, on 30 May 2017 at 20:04:30, subject to the Cambridge Core terms of use, available at https://www.cambridge.org/core/terms.
https://doi.org/10.1557/JMR.2005.0160

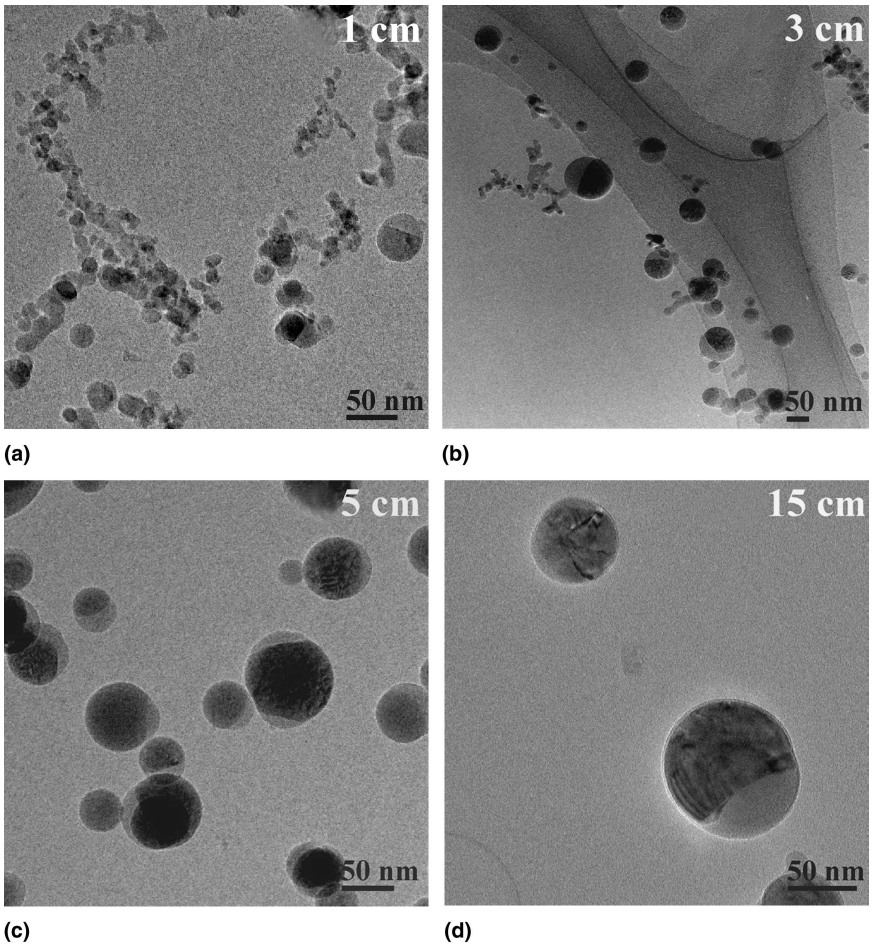

FIG. 6. TEM images of nanoparticles with 80 wt% TiO_2 collected by thermophoretic sampling at (a) 1 cm, (b) 3 cm, (c) 5 cm, and (d) 15 cm above the burner. The evolution of the silica-coated product particles at various flame heights can be observed.

flame [Fig. 6(a)] deposits upon collision on the surface of the spherical TiO_2 particles. If collisions between silica and titania particles take place at the flame edge or high up in the flame (HAB > 5 cm), silica particles may have grown too large and/or the temperature is too low for complete coalescence on the titania surface [Fig. 6(d)]. Thermophoretic sampling indicates that coating in this co-flow diffusion flame is consistent with that in counter-flow[16] diffusion flames; the dominant coating mechanism is the deposition of silica on the titania particle surface followed by fusion. The quality of the coating depends on the HAB where the collision of silica with titania occurs, as was indicated by sampling at 5 cm HAB.

Some 80 wt% TiO_2 particles collected at HAB = 15 cm were further investigated by STEM and EDX (Fig. 7). Figure 7(a) shows a single, fully coated particle: at positions 1 and 3 near the particle edges, silicon but no titanium is detected, confirming that the particle coating seen by TEM [Fig. 6(d)] is pure silica. At position 2 in the center of the particle both silicon and titanium are detected as the silica coating layer and the titania core are detected. For the particle with two segregated regions [Fig. 7(b)], only titanium was detected at position 3, while in the center of the darker area of the particle only silicon gives a signal (position 1). At the interface between the two regions, both silicon and titanium are detected (position 2).

3. Effect of composition on particle size and crystallinity

Figure 8 depicts the BET-equivalent diameter (circles), anatase crystallite size (triangles), and phase composition (squares) of particles produced without the flame-quenching nozzle (filled symbols) as a function of composition. The pure TiO_2 particles are larger (d_{BET} = 70 nm) than those of silica (d_{BET} = 33 nm) made at the same mass production rate because the former flame is hotter than the latter (Fig. 2) and TiO_2 sinters faster than SiO_2.[39] The BET particle diameter is 43 nm for 20 wt% TiO_2 and 52 nm for 40 wt% TiO_2. The increase in BET sizes with increasing TiO_2 content is consistent with Akhtar et al.[15] and Vemury and Pratsinis.[17] However, no difference in BET diameter was observed for

Downloaded from https://www.cambridge.org/core. University of Basel Library, on 30 May 2017 at 20:04:30, subject to the Cambridge Core terms of use, available at https://www.cambridge.org/core/terms.
https://doi.org/10.1557/JMR.2005.0160

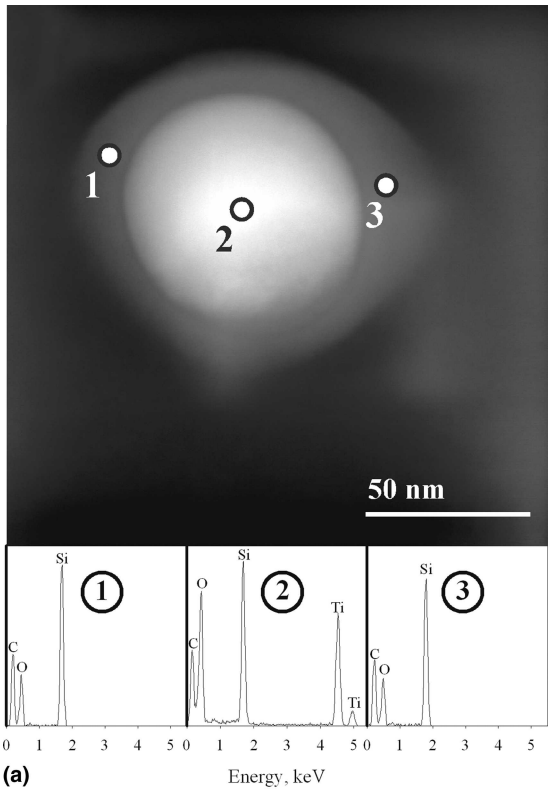

FIG. 7. STEM image and EDX analysis of particles with 80 wt% TiO_2 collected by thermophoretic sampling at 15 cm above the burner. Positions (1, 2, 3) for EDX analysis are marked in the STEM images. The titania particle in image (a) is encapsulated by silica, and the particle in image (b) has two segregated regions of silica and titania fused together at an interfacial region.

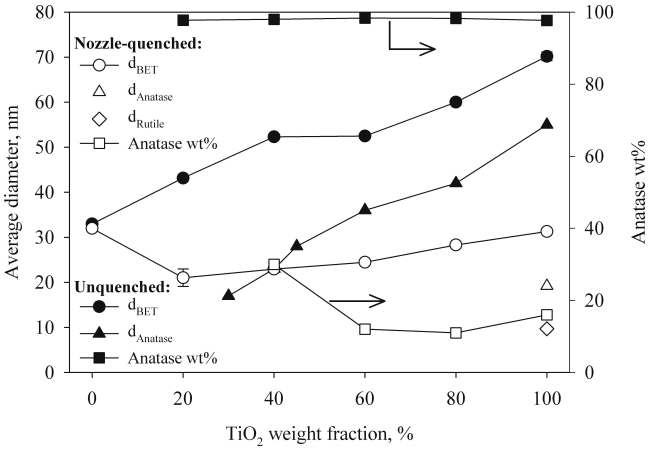

FIG. 8. BET-equivalent diameter (circles, left axis), anatase (triangles, left axis), and rutile (diamonds, left axis) sizes and anatase weight fraction (squares, right axis) of product particles as a function of the composition (weight percent TiO_2) made in the unquenched flame (filled symbols) and nozzle-quenched flame (open symbols). The BET-diameters are nearly halved by nozzle-quenching. In the unquenched flame titania is in all cases pure anatase, while nozzle-quenching promotes rutile formation.

powders containing 40 and 60 wt% TiO_2 consistent with Lee et al.[22] as particle growth is suppressed by homogenization of the two oxides. At 80 wt% TiO_2 the BET particle diameter has increased to 60 nm.

Figure 8 shows that all powders were >97 wt% anatase, independent of composition. The formation of anatase is characteristic for pure titania made from TTIP in oxygen-rich diffusion flames.[25] It has been shown also that the presence of silica during flame synthesis of titania promotes anatase formation.[17] When the titania content is decreased, the anatase crystallite size decreases in agreement with TEM observations [Figs. 4(c) and 4(d)]. Pure titania has an average crystallite size of 55 nm, e.g., about 15 nm smaller than the BET-equivalent particle diameter, indicating polycrystalline particles. At 60 wt% TiO_2, the anatase crystallites are 36 nm; at 40 wt% TiO_2 they have further decreased to 23 nm. The crystallite sizes decrease as a result of the reduced titania (precursor) concentration in the flame, and possibly also by the reduction of the sintering rate of titania in the presence of silica.[15]

C. Nozzle-quenched flame synthesis of SiO_2/TiO_2

1. Effect of composition of particle morphology

Figure 9 shows TEM images of (a,f) the pure oxide powders and the ones containing (b) 20 wt%, (c) 40 wt%, (d) 60 wt%, and (e) 80 wt% TiO_2 produced with the quenching nozzle at HAB = 5 cm. Particles of all compositions are spherical or nearly spherical with a low degree of agglomeration. This is in agreement with thermophoretic sampling of spherical particles at 5 cm HAB in the flame producing 80 wt% TiO_2 powders without the nozzle [Fig. 6(c)].

Downloaded from https://www.cambridge.org/core. University of Basel Library, on 30 May 2017 at 20:04:30, subject to the Cambridge Core terms of use, available at https://www.cambridge.org/core/terms.
https://doi.org/10.1557/JMR.2005.0160

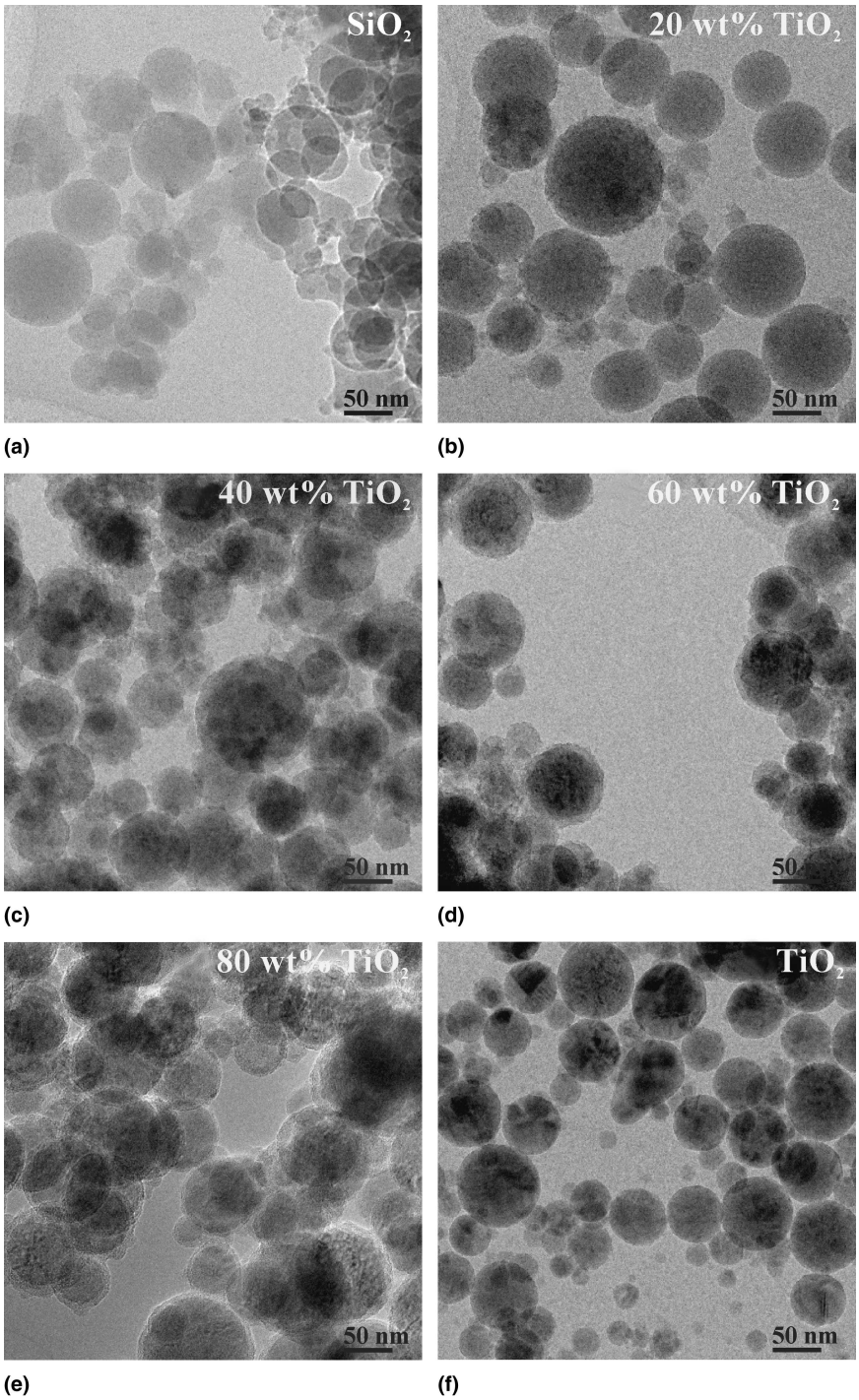

FIG. 9. TEM images of (a) pure silica, (b) 20 wt% TiO_2, (c) 40 wt% TiO_2, (d) 60 wt% TiO_2, (e) 80 wt% TiO_2, and (f) pure titania produced with the quenching nozzle placed at 5 cm above the burner. Silica-coated titania particles are formed at 60 and 80 wt% TiO_2.

At 40 wt% TiO_2 darker regions on some of the particles can be seen [Fig. 9(c)]. Figures 10(a)–10(c) shows elemental maps of these particles. Silicon and titanium appear light in the Si and Ti maps [Figs. 10(b) and 10(c)], respectively. The mapping indicates spotty titania regions on silica particles [Fig. 10(c)], but also individual particles of either pure silica or pure titania are detected. In contrast when these particles were made without the nozzle, they were segregated in amorphous silica and crystalline titania regions [Fig. 4(c)]. For the latter particles the high temperature residence time is long enough to reach the thermodynamically favorable state of large separate SiO_2 and TiO_2 phases (Fig. 4). However, when the nozzle is used, and the flame is rapidly quenched, the

Downloaded from https://www.cambridge.org/core. University of Basel Library, on 30 May 2017 at 20:04:30, subject to the Cambridge Core terms of use, available at https://www.cambridge.org/core/terms.
https://doi.org/10.1557/JMR.2005.0160

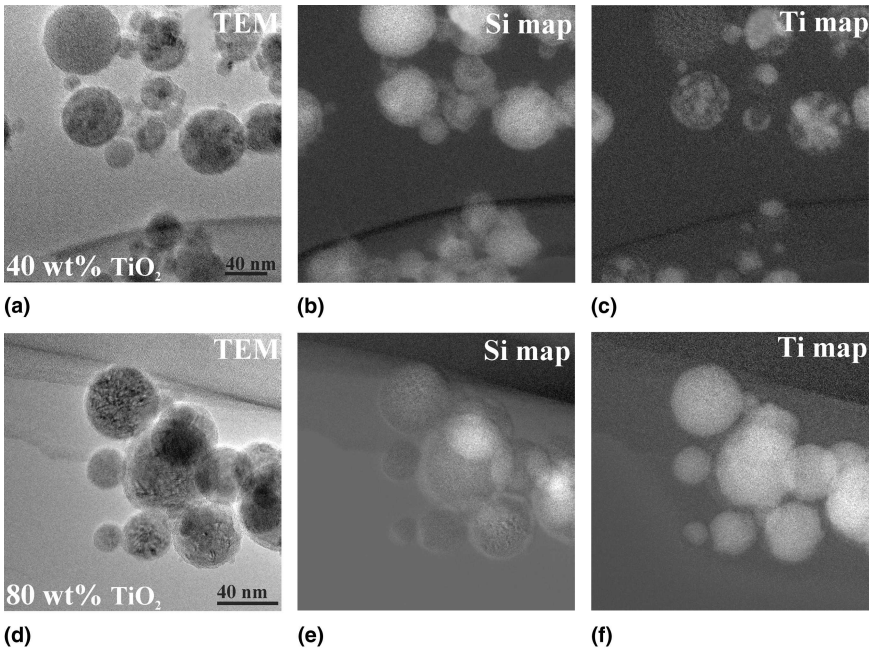

FIG. 10. Si and Ti maps and the corresponding TEM images of particles with (a–c) 40 wt% TiO_2 and (d–f) 80 wt% TiO_2. At 40 wt% TiO_2, spotty regions of titania on silica, as well as separate silica and titania particles are observed; particles at 80 wt% TiO_2 are encapsulated by silica.

lowest energy and thermodynamically most favorable state are not reached. As a result, TiO_2 particles are captured on the SiO_2 surface as they arrived without having a chance of surface diffusion and agglomeration forming large TiO_2 domains or islands as shown in Fig. 4(c).

The 60 wt% TiO_2 particles made with the nozzle [Fig. 9(d)] are coated with rough, inhomogeneous silica layers 3–12 nm thick. In contrast, without the nozzle, no coating layers were obtained at this composition, but segregated crystalline and amorphous regions were observed [Fig. 4(d)]. The formation of a coating at this composition with the nozzle again indicates that particles are frozen before reaching the thermodynamically dictated morphology of large SiO_2 islands on the TiO_2 surface.

The 80 wt% TiO_2 particles produced with the nozzle have smooth silica coatings 3–6 nm thick [Fig. 9(e)] as verified by elemental mapping [Figs. 10(d)–10(f)]. Silica encapsulates the titania particles as a lighter (Si) tone is seen at their fringes [Fig. 10(e)]. The white spots in the center of some of the particles come from externally overlapping particles. The titania particles appear white in the Ti-map [Fig. 10(f)], however the fringes of the particles are dark. These dark areas correspond to the light areas detected in the silicon map [Fig. 10(e)], e.g., confirming that the titania particles are encapsulated by a layer of silica. This was also verified by EDX analysis, as was shown in Fig. 7(a) for these particles prepared without the quenching nozzle. Here in the particle center mainly titanium is detected by EDX, while the silicon concentration increases moving the EDX probe towards the edge of the particle.

Thinner and more homogeneous SiO_2 coatings were formed on the 80 wt% TiO_2 [Fig. 9(e)] than on the 60 wt% TiO_2 particles [Fig. 9(d)] as it would be expected by a mass balance. This is consistent again with Powell et al.[19] who formed denser and smoother silica coatings on titania in a hot-wall reactor by decreasing the silica precursor concentration. A decrease in HDMSO concentration should result in the formation of smaller silica particles, which have a better chance to collide with the newly formed TiO_2 rather than by themselves. Furthermore, their smaller size facilitates their sintering and formation of a coating upon collision. The rapid cooling by nozzle quenching may have prevented silica mobility on the titania surface that would have resulted in segregated SiO_2 domains or islands.

The growth of the 80 wt% TiO_2 particles upstream of the nozzle is essentially the same with that seen without the nozzle [Fig. 5(b)]. The flame temperature profile is not influenced by the nozzle up to 4 cm HAB (Fig. 2) and the precursor concentrations as well as the gas flow rates are identical. In Fig. 6(c), it was shown that at 5 cm HAB titania particles are partly coated by silica. By placing the nozzle at this position, total silica encapsulation of the titania particles is achieved [Fig. 9(e)]. This suggests that silica freezes on the titania surface during quenching, forming a homogeneous coating layer. Without flame quenching, particle collisions will still take place at HAB > 5 cm. Segregated or inhomogeneously coated particles are formed by silica-titania particles colliding in these colder parts of the flame [Fig. 4(e)].

Downloaded from https://www.cambridge.org/core. University of Basel Library, on 30 May 2017 at 20:04:30, subject to the Cambridge Core terms of use, available at https://www.cambridge.org/core/terms.
https://doi.org/10.1557/JMR.2005.0160

2. Effect of composition on particle size and crystallinity

Figure 8 shows the BET-equivalent diameter (circles), the anatase (triangles), and rutile (diamonds) sizes and phase composition (squares) of particles produced with the quenching nozzle (open symbols) as a function of composition. The BET diameter of pure titania was reduced to 31 nm with the nozzle, compared to 70 nm without the nozzle consistent with Wegner and Pratsinis.[25] Pure silica has a BET diameter of 32 nm, similar to that obtained without the nozzle. This indicates that silica particle growth (by coagulation and sintering) was completed at earlier flame stages and is not affected by nozzle quenching. At the used temperatures and particles sizes, the sintering rate of SiO_2 is slower[41] than that of TiO_2. For the silica/titania powders, the BET particle diameters were about half that of the ones obtained without the nozzle. For example, at 60 wt% TiO_2 the BET diameters were 24 and 52 nm with and without the nozzle, respectively. The particle sizes increase with increasing TiO_2 content. This trend is less pronounced than in the unquenched flame (Fig. 8), as the particle residence time at high temperatures is shorter in the nozzle-quenched flame thereby significantly reducing particle growth by sintering.

Pure titania made with the nozzle has a rutile content of 84 wt% and the balance anatase (16 wt%) with anatase and rutile sizes of 19.2 and 9.7 nm, respectively (Fig. 8). These crystallite sizes are smaller than the BET diameter, indicating polycrystalline titania, as was also observed in the unquenched flame. The rutile content decreases with increasing residence time in the flame,[25] as rutile formation is promoted by oxygen vacancies, which are created at low oxygen partial pressures. The oxygen partial pressure increases with increasing flame length, as more oxygen diffuses into the core region of the flame and therefore pure anatase powders are produced without the nozzle (Fig. 8). The powders produced with the quenching nozzle exhibited a bluish coloration characteristic for oxygen-deficient titania.[25]

Upon addition of silica, the rutile content is constant for up to 60 wt% TiO_2; at 40 wt% TiO_2, the anatase content has increased to 30 wt%. This indicates that with increasing SiO_2 concentration, silica inhibits the anatase to rutile transformation as Si^{4+} is small enough to enter the titania lattice interstitially.[15] At 20 wt% TiO_2 the titania crystal phases are no longer visible in the XRD spectra, and only amorphous phases are detected.

IV. CONCLUSIONS

Silica/titania nanoparticles were made in co-flow diffusion flames by co-introduction of silicon and titanium precursors. Silica-coated spherical titania particles could be produced at high weight fractions of titania. Filamentary silica deposits on the titania particle surface and sinters as it passes through the high-temperature region of the flame forming a coating layer or segregated silica islands depending on the particle cooling rate. The morphology, as well as the crystallinity of the silica/titania particles, could be further controlled by rapidly freezing particle growth by aerosol expansion through a critical flow nozzle above the flame. This fast cooling facilitated synthesis of rather smooth silica coatings by essentially freezing silica surface diffusion and rearrangement on the titania particle surface. Furthermore, nozzle quenching promoted rutile formation by reducing oxygen diffusion at high temperatures, even in the presence of the anatase-promoter silica.

ACKNOWLEDGMENTS

Financial support by the Swiss National Science Foundation (No. 200021-100325) and the Swiss Comission for Technology and Innovation (TopNano 21, No. 6740.1 TNS) is acknowledged.

REFERENCES

1. G.D. Ulrich: Flame synthesis of fine particles. *Chem. Eng. News* **62,** 22 (1984).
2. J.H. Braun: Titanium dioxide—A review. *J. Coat. Technol.* **69,** 59 (1997).
3. R.J. Nussbaumer, W.R. Caseri, P. Smith, and T. Tervoort: Polymer-TiO_2 nanocomposites: A route towards visually transparent broadband UV filters and high refractive index materials. *Macromol. Mater. Eng.* **288,** 44 (2003).
4. J. Lademann, H.J. Weigmann, H. Schafer, G. Muller, and W. Sterry: Investigation of the stability of coated titanium microparticles used in sunscreens. *Skin Pharmacol. Appl. Skin Physiol.* **13,** 258 (2000).
5. J. Winkler: Nano-scaled titanium dioxide—properties and use in coatings with special functionality. *Macromol. Symp.* **187,** 317 (2002).
6. U. Gesenhues: Contribution of TiO_2 to the durability and the degradation of organic coatings. *Double Liaison* **43,** 32 (1996).
7. T. Picatonotto, D. Vione, and M.E. Carlotti: Effect of some additives used in the cosmetic field on the photocatalytic activity of rutile. *J. Dispersion Sci. Technol.* **23,** 845 (2002).
8. R.K. Iler: Product comprising a skin of dense, hydrated amorphous silica bound upon a core of another solid material and process of making same. U.S. Patent No. 2 885 366 (1959).
9. A.J. Werner: Titanium dioxide pigment coated with silica and alumina. U.S. Patent No. 3 437 502 (1969).
10. S.P. Kinniard and A. Campeotto: Method for manufacturing high opacity, durable pigments. U.S. Patent No. 6 528 568 B2 (2003).
11. S.M. Herkimer: Process for manufacturing titanium dioxide pigment having a hydrous oxide coating using a media mill. U.S. Patent No. 5 730 795 (1998).
12. T.A. Egerton: The modification of fine powders by inorganic coatings. *KONA* **16,** 46 (1998).

Downloaded from https://www.cambridge.org/core. University of Basel Library, on 30 May 2017 at 20:04:30, subject to the Cambridge Core terms of use, available at https://www.cambridge.org/core/terms. https://doi.org/10.1557/JMR.2005.0160

13. L. Piccolo, B. Calcagno, and E. Bossi: Process for the post-treatment of titanium dioxide pigments. U.S. Patent No. 4 050 951 (1977).
14. E. Santacesaria, S. Carra, R.C. Pace, and C. Scotti: Vapor-phase treatment of titanium-dioxide with metal chlorides 1. The reactions of coating performed by Al_2Cl_6, $SiCl_4$, and $ZrCl_4$ in the vapor-phase. *Ind. Eng. Chem. Prod. Res. Dev.* **21,** 496 (1982).
15. M.K. Akhtar, S.E. Pratsinis, and S.V.R. Mastrangelo: Dopants in vapor-phase synthesis of titania powders. *J. Am. Ceram. Soc.* **75,** 3408 (1992).
16. C.H. Hung and J.L. Katz: Formation of mixed-oxide powders in flames 1. TiO_2–SiO_2. *J. Mater. Res.* **7,** 1861 (1992).
17. S. Vemury and S.E. Pratsinis: Dopants in flame synthesis of titania. *J. Am. Ceram. Soc.* **78,** 2984 (1995).
18. T.T. Kodas, Q.H. Powell, and B. Anderson: Coating of TiO_2 pigment by gas-phase and surface reactions. International Patent No. WO 96/36441 (1996).
19. Q.H. Powell, G.P. Fotou, T.T. Kodas, B.M. Anderson, and Y.X. Guo: Gas-phase coating of TiO_2 with SiO_2 in a continuous flow hot-wall aerosol reactor. *J. Mater. Res.* **12,** 552 (1997).
20. S.H. Ehrman, S.K. Friedlander, and M.R. Zachariah: Characteristics of SiO_2/TiO_2 nanocomposite particles formed in a premixed flat flame. *J. Aerosol Sci.* **29,** 687 (1998).
21. S.H. Ehrman, S.K. Friedlander, and M.R. Zachariah: Phase segregation in binary SiO_2/TiO_2 and SiO_2/Fe_2O_3 nanoparticle aerosols formed in a premixed flame. *J. Mater. Res.* **14,** 4551 (1999).
22. S.K. Lee, K.W. Chung, and S.G. Kim: Preparation of various composite TiO_2/SiO_2 ultrafine particles by vapor-phase hydrolysis. *Aerosol Sci. Technol.* **36,** 763 (2002).
23. W.J. Stark and S.E. Pratsinis: Aerosol flame reactors for manufacture of nanoparticles. *Powder Technol.* **126,** 103 (2002).
24. K. Wegner, W.J. Stark, and S.E. Pratsinis: Flame-nozzle synthesis of nanoparticles with closely controlled size, morphology and crystallinity. *Mater. Lett.* **55,** 318 (2002).
25. K. Wegner and S.E. Pratsinis: Nozzle-quenching process for controlled flame synthesis of titania nanoparticles. *AIChE J.* **49,** 1667 (2003).
26. H.K. Kammler, S.E. Pratsinis, P.W. Morrison, and B. Hemmerling: Flame temperature measurements during electrically assisted aerosol synthesis of nanoparticles. *Combust. Flame* **128,** 369 (2002).
27. H.K. Kammler, R. Jossen, P.W. Morrison, S.E. Pratsinis, and G. Beaucage: The effect of external electric fields during flame synthesis of titania. *Powder Technol.* **135,** 310 (2003).
28. R.W. Cheary and A. Coelho: A fundamental parameter approach to x-ray line-profile fitting. *J. Appl. Crystallogr.* **25,** 109 (1992).
29. T.E. Daubert, R.P. Danner, H.M. Sibul, and C.C. Stebbins: *Physical and Thermodynamic Properties of Pure Chemicals: Data Compilation*, Design Institute for Physical Property Data, American Institute of Chemical Engineers; NSRDS, National Standard Reference Data System (Taylor & Francis, New York, NY, 1997).
30. R. Mueller, H.K. Kammler, S.E. Pratsinis, A. Vital, G. Beaucage, and P. Burtscher: Non-agglomerated dry silica nanoparticles. *Powder Technol.* **140,** 40 (2004).
31. K.H. Ahn, Y.B. Park, and D.W. Park: Kinetic and mechanistic study on the chemical vapor deposition of titanium dioxide thin films by in situ FTIR using TTIP. *Surf. Coat. Technol.* **171,** 198 (2003).
32. P.W. Morrison, R. Raghavan, A.J. Timpone, C.P. Artelt, and S.E. Pratsinis: In situ Fourier transform infrared characterization of the effect of electrical fields on the flame synthesis of TiO_2 particles. *Chem. Mater.* **9,** 2702 (1997).
33. A.Y. Stakheev, E.S. Shpiro, and J. Apijok: XPS and XAES Study of TiO_2-SiO_2 mixed-oxide system. *J. Phys. Chem.* **97,** 5668 (1993).
34. M. Anpo, T. Shima, S. Kodama, and Y. Kubokawa: Photocatalytic hydrogenation of CH_3CCH with H_2O on small-particle TiO_2–Size quantization effects and reaction intermediates. *J. Phys. Chem.* **91,** 4305 (1987).
35. G. Lassaletta, A. Fernandez, J.P. Espinos, and A.R. González-Elipe: Spectroscopic characterization of quantum-sized TiO_2 supported on silica: Influence of size and TiO_2–SiO_2 interface composition. *J. Phys. Chem.* **99,** 1484 (1995).
36. R.C. DeVries, R. Roy, and E.F. Osborn: The system TiO_2–SiO_2. *Trans. Brit. Ceram. Soc.* **53,** 525 (1954).
37. P.C. Schultz: Binary titania-silica glasses containing 10 to 20 wt% TiO_2. *J. Am. Ceram. Soc.* **59,** 214 (1976).
38. K. Nakaso, K. Okuyama, M. Shimada, and S.E. Pratsinis: Effect of reaction temperature on CVD-made TiO_2 primary particle diameter. *Chem. Eng. Sci.* **58,** 3327 (2003).
39. Y. Xiong and S.E. Pratsinis: Formation of agglomerate particles by coagulation and sintering 1. A 2-dimensional solution of the population balance equation. *J. Aerosol Sci.* **24,** 283 (1993).
40. Q.H. Powell, G.P. Fotou, T.T. Kodas, and B.M. Anderson: Synthesis of alumina- and alumina/silica-coated titania particles in an aerosol flow reactor. *Chem. Mater.* **9,** 685 (1997).
41. Y. Xiong, M.K. Akhtar, and S.E. Pratsinis: Formation of agglomerate particles by coagulation and sintering 2. The evolution of the morphology of aerosol-made titania, silica and silica-doped titania powders. *J. Aerosol Sci.* **24,** 301 (1993).

Downloaded from https://www.cambridge.org/core. University of Basel Library, on 30 May 2017 at 20:04:30, subject to the Cambridge Core terms of use, available at https://www.cambridge.org/core/terms.
https://doi.org/10.1557/JMR.2005.0160